Volatility of Sodium in Carbonaceous Chondrites at Temperatures Consistent with Low-perihelion Asteroids

Joseph R. Masiero[1] , Björn J. R. Davidsson[2], Yang Liu[2], Kelsey Moore[2], and Michael Tuite[2]

[1] Caltech/IPAC, 1200 E California Boulevard, MC 100-22, Pasadena, CA 91125, USA; jmasiero@ipac.caltech.edu
[2] Jet Propulsion Laboratory/California Institute of Technology, 4800 Oak Grove Drive, MS 183-301, Pasadena, CA 91109, USA

Abstract

Solar system bodies with surface and subsurface volatiles will show observational evidence of activity when they reach a temperature where those volatiles change from solid to gas and are released. This is most frequently seen in comets, where activity is driven by the sublimation of water, carbon dioxide, or carbon monoxide ices. However, some bodies (notably the asteroid (3200) Phaethon) show initiation of activity at very small heliocentric distances, long after they have reached the sublimation temperatures of these ices. We investigate whether the sodium present in the mineral matrix could act as the volatile element responsible for this activity. We conduct theoretical modeling which indicates that sodium has the potential to sublimate in the conditions that Phaethon experiences, depending on the mineral phase it is held in. To test this, we then exposed samples of the carbonaceous chondrite Allende to varying heating events, similar to what would be experienced by low-perihelion asteroids. We measured the change in sodium present in each sample and find that the highest temperature samples show a significant loss of sodium from specific mineral phases over a single heating event, comparable to a day on the surface of Phaethon. Under specific thermal histories possible for Phaethon, this outgassing could be sufficient to explain this object's observed activity. This effect would also be expected to be observed for other low-perihelion asteroids as well and may act as a critical step in the process of disrupting small low-albedo asteroids.

Unified Astronomy Thesaurus concepts: Asteroids (72); Near-Earth objects (1092); Comet volatiles (2162)

1. Introduction

The small bodies of the inner solar system are generally grouped into two phenomenological classes: comets and asteroids. The main difference distinguishing these two populations is whether or not the body is observed to show activity in the form of emission of gas and dust. This divide is usually traced to whether the object contains frozen subsurface volatile materials such as water, carbon dioxide, or carbon monoxide and therefore is used as a proxy for where in the solar system the object formed with respect to the proto-planetary ice line of each molecule.

Recently, this clear distinction has been called into question by a newly recognized population of objects. These objects, on asteroid-like orbits, have been seen to show comet-like activity (Jewitt et al. 2015). Referred to by various publications as Active Asteroids, Main Belt Comets, or Active Main Belt Objects, this population can be divided into objects showing activity from impact events, objects with activity consistent with disruption after rotational spin up, and objects with activity consistent with the presence of subsurface water ice.

However, there are a few objects that fail to fit into any of these broad categories. The most notable example is the asteroid (3200) Phaethon, a near-Earth object (NEO) that has been shown to be active at perihelion (Jewitt & Li 2010; Li & Jewitt 2013) and is orbitally associated with the Geminid meteor stream (Gustafson 1989). The perihelion of Phaethon is $q = 0.14$ au and its aphelion is $Q = 2.4$ au, making the surface temperatures on the day-lit side well above the sublimation temperature of water ice for the

majority of its orbit. Any ice thermally coupled to the surface would be expected to have been removed quickly after Phaethon's dynamical transfer into its current orbit, and not survive to the present day. MacLennan et al. (2021) have shown that over the course of its orbital evolution Phaethon has undergone numerous cycles through high peak temperatures like today, which would have baked off any water near the surface. This means water ice cannot be driving the observed activity, which is seen only in a short temporal period around Phaethon's perihelion. This short burst of activity would not be the behavior expected if water ice was driving the activity. While water could be bound up in hydrated silicates, experiments by Garenne et al. (2014) have shown that these minerals in meteorites begin losing mass below 873 K, well below Phaethon's perihelion temperature. Recent spectral observations by Takir et al. (2020) have indicated an absence of hydrated minerals on the surface, further supporting the conclusion that they are not the source of activity.

Previous investigations have looked into the effects of the extreme temperatures that Phaethon experiences at perihelion (Delbo et al. 2014; Ryabova 2018; Yu et al. 2019; MacLennan et al. 2021). These studies have found that fracturing, driven by thermal cycling, can efficiently fragment boulders with Phaethon's expected surface composition. This would act as a source of dust that could eventually be ejected from the surface to create the observed brightening and the associated meteor stream. However, thermal fracturing alone is unlikely to produce sufficient force to let this dust reach escape velocity and be emitted from Phaethon.

We propose that the driver of the activity on Phaethon at perihelion is the volatilization of sodium bound in minerals such as sodalite and nepheline distributed in the matrix. Other than water ice, which was lost early during Phaethon's transition to a near-Earth orbit, sodium is one of the most volatile elements present at a significant quantity in asteroidal

Table 1
Orbital, Rotational, and Physical Parameters Applied in the Thermophysical Model of Phaethon

Symbol	Description	Value	Unit	Reference
a	Semimajor axis	1.271 36	au	MPC
e	Eccentricity	0.889 849 5	…	MPC
i	Inclination	22.259 64	°	MPC
ω	Argument of perihelion	322.186 86	°	MPC
Ω	Longitude of the ascending node	265.217 48	°	MPC
$\mathcal{T}$	Perihelion date	2 459 191.093 586 5	JD	MPC
P	Rotation period	3.603 958	h	Hanuš et al. (2016)
λ	Spin axis ecliptic longitude	319	°	Hanuš et al. (2016)
β	Spin axis ecliptic latitude	−39	°	Hanuš et al. (2016)
D	Diameter	4.6	km	Masiero et al. (2019)
A	Bond albedo	0.04	…	Golubeva et al. (2020)
ε	Emissivity	0.9	…	
ρ_{sil}	Silicate grain density	3000	kg m^{-3}	Macke et al. (2011)
ρ_{Na}	Sodium grain density	968	kg m^{-3}	
ψ	Porosity	0.5	…	
m_{Na}	Sodium abundance	0.5	wt%	Lodders (2003)
r_g	Grain radius	100	μm	
L_t	Tube length	1	mm	
r_t	Tube radius	100	μm	
ξ	Tortuosity	1	…	
T_0	Initial temperature	260	K	

Note. MPC is the Minor Planet Center (https://minorplanetcenter.net).

materials (Notsu et al. 1978; Asplund et al. 2009; Sossi & Fegley 2018). Mercury, with a perihelion of $q = 0.31$ au, is known to have an exosphere populated by vaporized sodium (Cassidy et al. 2015), which means that sodium volatilization does occur in the near-Sun region. It is important to note that Cassidy et al. (2015) show that the temperature profile of Mercury's exosphere implies that the primary mechanism of volatilization is photon-stimulated desorption instead of thermalization. They attribute the lack of thermalized sodium to space weathering, which we would expect to be less significant for Phaethon given that it is a dynamically much younger object.

Additionally, the Geminid meteors have been observed to be depleted in sodium compared to other meteor streams (Kasuga et al. 2005; Abe et al. 2020). Kasuga et al. (2006) investigated the sodium content of meteor showers, finding that while the current orbit of Phaethon does not reach the condensation temperatures for common sodium minerals such as feldspar, small particles will experience higher temperatures and may be devolatilized that way. They suggest that the submillimeter-scale Geminid meteors were depleted in sodium after being ejected from the parent body. However, we propose here the converse: that it is the devolatilization of sodium-bearing minerals on Phaethon that prompted the ejection of the particles that became the Geminids, and thus they were sodium-depleted during their formation.

To investigate this hypothesis, we conducted thermophysical modeling of Phaethon as it orbits the Sun to determine the feasibility of this mechanism. We then performed heating experiments on meteorite samples as an analog for Phaethon to search for sodium loss. Sodium content was determined for a range of peak heating temperatures on individual minerals within each sample, which were analyzed post-heating for changes to their chemistry. This work is intended to be an initial look into the possibility of sodium volatilization causing

activity on low-perihelion bodies, and future work will constrain this effect in further detail.

2. Thermophysical Modeling of Phaethon

To test the feasibility of our hypothesis that sodium sublimation is driving the activity of Phaethon, we performed thermophysical modeling of that process. We consider Phaethon as a spherical, rotating, and orbiting body consisting of a porous mixture of silicate and sodium grains. Constant model parameters are provided in Table 1. We apply the thermophysical model NIMBUS (Numerical Icy Minor Body evolUtion Simulator) developed by Davidsson (2021; see also Davidsson et al. 2021). NIMBUS considers a number of latitudinal slabs (here 18, evenly distributed in cosine), each split into a number of radial cells, stretching from the body center to the surface (here 123 cells, with a thickness of 200 m at the core, diminishing with geometric progression to 0.003 m at the surface). For this grid, NIMBUS solves a coupled system of differential equations that govern the radial and latitudinal transport of heat and mass throughout the body. The upper boundary condition of the energy conservation equation balances absorbed solar radiation (calculated as a function of orbital position, latitude, and rotational phase) with thermal reradiation into space and heat conducted to or from the surface. At depth, the energy conservation equation accounts for solid-state conduction, radiative transfer of energy in pores, energy consumption of sublimating solid sodium, energy transport (advection) of diffusing vaporized sodium, and energy release when vaporized sodium recondenses into a solid. We note that here we use diffusion to refer to gas flowing through an empty channel (e.g., pore space within the body), as opposed to atomic transport within solids, which we will refer to as "Fickian diffusion." The mass conservation equation ensures that vapor diffuses according to local temperature and pressure gradients, tracks the withdrawal of the sodium
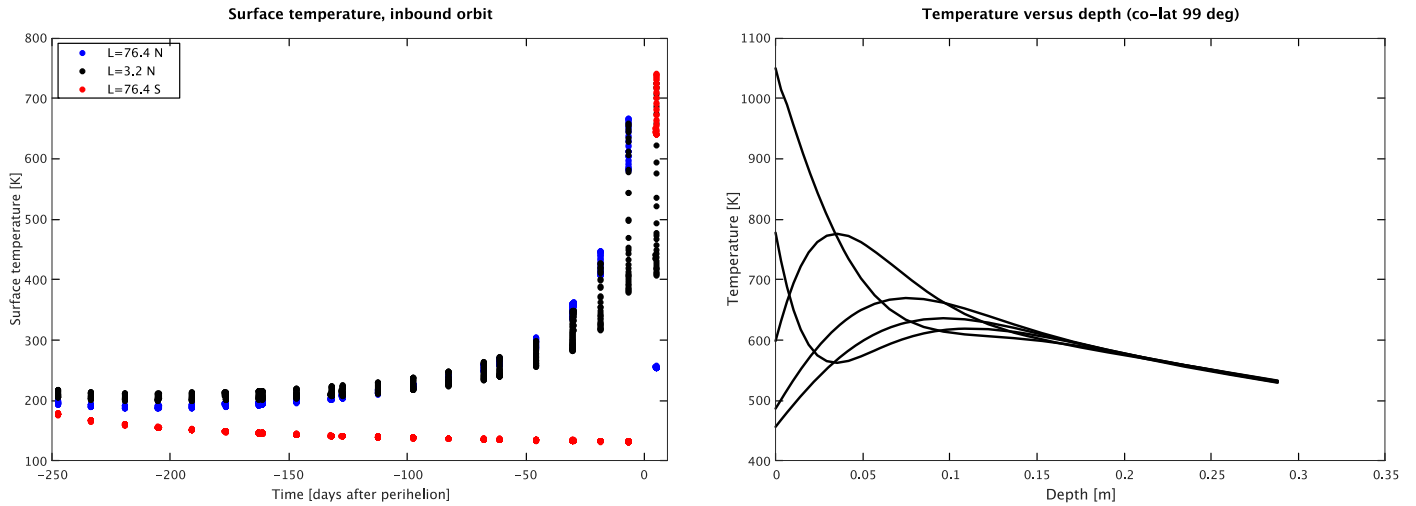
Figure 1. Left: surface temperature at three specific latitudes as a function of time from aphelion to perihelion. The vertical extension of data point clusters illustrates the range of day–night temperature variations. One rotation period every second week is plotted for clarity. Right: temperature as a function of depth for a handful of rotational phases, valid at perihelion for latitude 9° S. Note that this particular revolution is not plotted in the left figure.

sublimation front below the surface, and regulates the release of vaporized sodium into space.

A number of temperature-dependent and material-specific functions are used by NIMBUS to regulate the behavior of the physical processes under consideration. For the heat capacity $c = c(T)$ of both rock and sodium, it uses forsterite (Mg_2SiO_4) as an analog, as measured by Robie et al. (1982). The heat conductivity of compacted material $\kappa = \kappa(T)$ is taken as that of the H5 ordinary chondrite Wellman measured by Yomogida & Matsui (1983). Because it has been suggested that CK4 carbonaceous chondrites are Phaethon analogs (Clark et al. 2010), we apply the whole-rock density $\rho_{sil} = 3000$ kg m^{-3} as measured for such meteorites (Macke et al. 2011). We correct the heat conductivity for porosity ψ by applying the generation $n = 2$ Hertz factor $h = h(\psi)$ function of Shoshany et al. (2002). This allows us to calculate an instantaneous thermal inertia,

$$\Gamma = \sqrt{c(T)\rho(1 - \psi)\kappa(T)h(\psi)}. \qquad (1)$$

Trial runs indicated that $\psi = 0.5$ would yield $670 \lesssim \Gamma \lesssim 1000$ J m^{-2} s$^{-0.5}$ K^{-1} for the surface temperature range experienced by Phaethon. This is similar to the $\Gamma = 600 \pm 200$ J m^{-2} s$^{-0.5}$ K^{-1} range measured for Phaethon by Hanuš et al. (2016) and the $\Gamma = 880^{+580}_{-330}$ J m^{-2} s$^{-0.5}$ K^{-1} range measured for Phaethon by Masiero et al. (2019), which motivates our choice of porosity.

To describe sodium sublimation we applied the latent heat and Hertz–Knudsen formula parameters tabulated by Huebner (1970), which allowed us to define the corresponding saturation partial pressure ([Pa]) of sodium vapor above metallic sodium:

$$p_{sat}(T) = 10^{1.7372 \cdot (\mathcal{L} - 10)} 10^{\alpha - \beta L/T} \sqrt{\frac{2 \cdot 10^{-3}\pi k_B}{N_A}}, \qquad (2)$$

where $\alpha = 29.770$ and $\beta = 0.21860$ are constants, $L = 2.46 \cdot 10^4$ cal mole^{-1} is the latent heat, $\mathcal{L} = L/R_0 T_s = 10.8$ (where R_0 is the universal gas constant and T_s is the sodium boiling temperature), k_B is the Boltzmann constant, and N_A is the Avogadro constant (Huebner 1970). Whenever the local partial pressure of sodium vapor is below $p_{sat}(T)$ it will trigger sublimation if solid sodium is present. Conversely, sodium gas will recondense where the local partial pressure exceeds $p_{sat}(T)$.

We consider pure sodium here as the limiting case for what is occurring on Phaethon; in reality any sodium would initially be contained in a silicate mineral phase. The volume mass sublimation and condensation rates are calculated using standard expressions (e.g., Mekler et al. 1990; Prialnik 1992; Tancredi et al. 1994). Gas diffusion fluxes are calculated using the Clausing formula, evaluated as in Davidsson & Skorov (2002). These expressions require a number of geometrical parameters (r_g, L_t, r_t, ξ), for which we apply educated guesses (Table 1). At the modeled sublimation rate, the solution is not strongly sensitive to the diffusivity value that results from these geometrical parameters, as discussed by Davidsson (2021). If the diffusivity changes, the temperature and pressure profiles adjust in such a way that the same net mass-loss rate takes place and the same latent energy is being consumed.

The simulation was initiated at aphelion ($Q = 2.40$ au), assuming an initial temperature $T_0 = 260$ K, and terminated after the following perihelion ($q = 0.14$ au). This provided sufficient time for the near-surface region to lose memory of the arbitrary initial conditions. We also assumed that the (chondritic) sodium abundance m_{Na} initially was constant throughout the body.

Figure 1 shows that the surface temperature remains below $\sim$300 K at all latitudes, except during a four-month period around perihelion. Within four weeks of perihelion, the peak temperature exceeds $\sim$700 K and briefly reaches a maximum of 1050 K near the equator in the upper few centimeters of regolith as shown on the right in Figure 1. These results are comparable to a recently published thermophysical analysis of Phaethon by MacLennan et al. (2021) and Abe et al. (2020). Interestingly, the spin axis is oriented such that the northern hemisphere is illuminated up to perihelion. The equinox occurs close to this point, which keeps the south pole dark and cold until it suddenly receives substantial illumination. The drastic temperature jump of the south pole from nearly 100 K to above 700 K over the course of a week could potentially explain the surge of activity seen near perihelion (Jewitt & Li 2010; Li & Jewitt 2013).

Figure 2 shows that the temperatures experienced by Phaethon are sufficiently high to cause significant sodium volatilization if the element is present in pure form. Within $\sim$1 au of the Sun, the
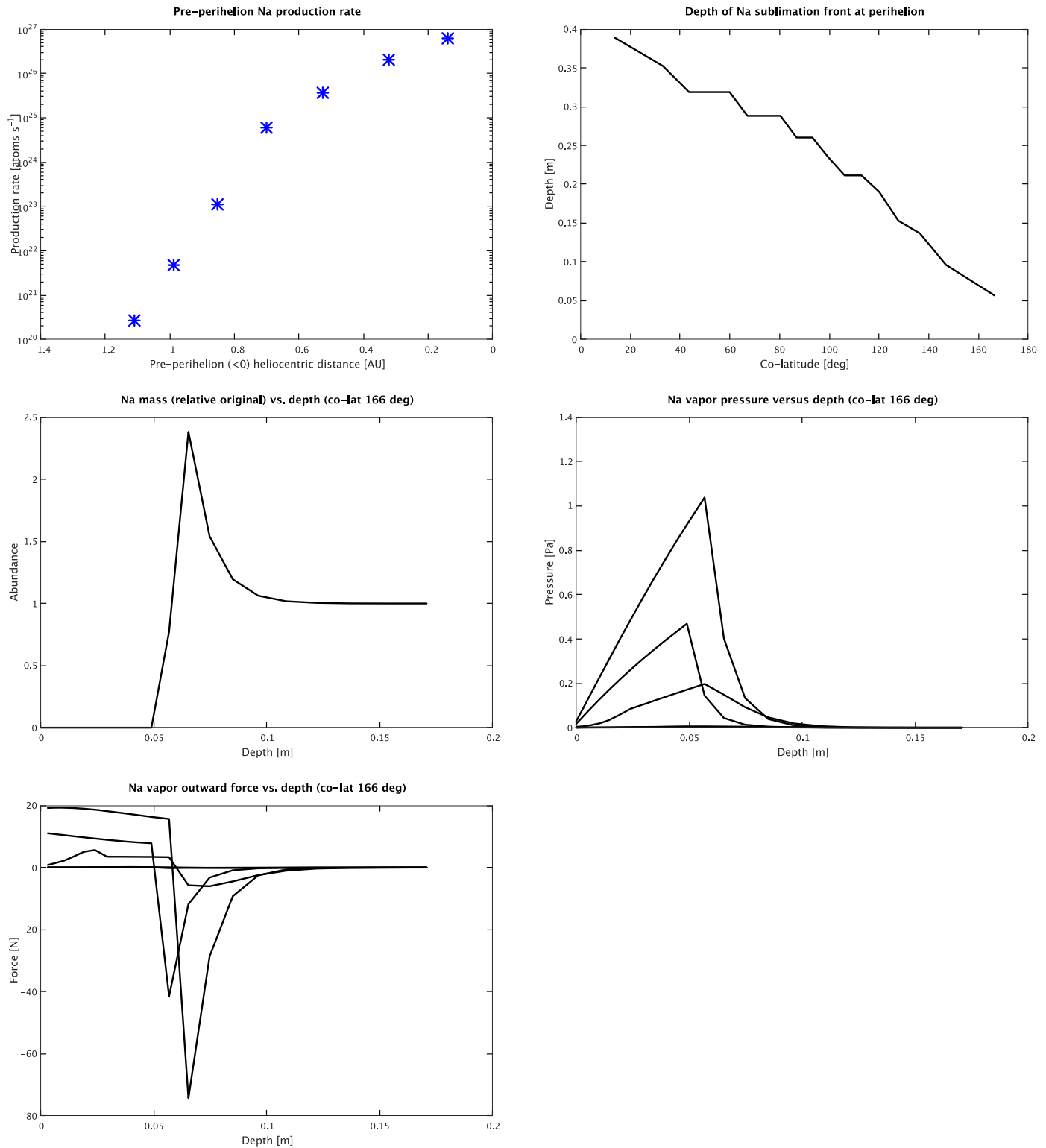
Figure 2. Upper left: the total sodium production rate calculated for Phaethon, as a function of heliocentric distance within ∼1 au of the Sun (from 45 days pre-perihelion). Upper right: the location of the sodium sublimation front as a function of the angular distance from the north pole (the colatitude) at perihelion. Middle left: the sodium abundance as a function of depth at latitude 76° S at perihelion, normalized to the initial abundance. Middle right: the pressure created by sodium volatilization as a function of depth for a few rotational phases for 76° S at perihelion. Lower left: the corresponding force caused by the sodium pressure gradient shown in the middle right figure.

sodium production rate increases six orders of magnitude, briefly reaching a molar perihelion production rate that parallels the water production rate of Comet 67P/Churyumov–Gerasimenko at 2.1 au (Fougere et al. 2016). If pure sodium were present and such strong outgassing takes place on Phaethon, it would readily cause comet-like ejection of dust into space. Figure 2 shows that the sodium sublimation front withdraws rapidly below the surface, reaching a depth of 0.4 m at the north pole at perihelion. The

simulation did not explicitly model the erosion of the surface because of comet-like activity, therefore these depths should be considered upper limits on the front withdrawal per orbit.

The pressure peak at the subsurface sublimation front forces sodium vapor to flow both outward and inward. The outward flow is responsible for the outgassing into space, whereas vapor flowing inwards eventually reaches colder material and recondenses. This causes a gradual build-up of sodium at depth. The NIMBUS simulations show that local concentrations that are at least twice as high as the original abundance can form. Such redistribution of solid sodium, especially when occurring slowly over time and when combined with impacts that expose deeper layers to space, could cause strong episodic bursts of activity. Figure 2 also shows the force $F = -dp/dr\ \hat{r}$ caused by the pressure variation $p = p(r)$ with the radial coordinate r. The outward force here reaches a peak of ~ 20 N. Given the low surface gravity of Phaethon ($g \approx 0.001\,\mathrm{m\,s^{-2}}$), such a force would be capable of lifting meter-sized boulders. Note that these results assume a pure sodium phase just below the surface and thus are meant to represent a bounding case.

Pure sodium is not common in carbonaceous chondrites and most of the element is hosted by minerals like feldspar, nepheline $[(Na,K)AlSiO_4]$, sodalite, and saponite (Rubin 1997). However, there are at least two mechanisms that could segregate sodium from the host and create a pure phase in bodies like Phaethon that come unusually close to the Sun. First, Čapek & Borovička (2009) assembled atomic diffusivity data for sodium for a range of relevant minerals and demonstrated that substantial Fickian diffusion could occur at temperatures reached by Phaethon on timescales similar to the orbital period, if the grains are sufficiently small. Heating of material at depths from which vapor transport to the surface is limited could build a pure sodium deposit over time as the sodium gas cools and condenses to a solid phase, which later could become exposed at the surface by, e.g., cratering or landslides. Second, laboratory experiments by Russell & Sanders (1994) showed that layers of pure sodium formed on the surface of NaCl particles when irradiated with 0.5 keV electrons. Solar wind electrons typically reach 10–50 eV, but superhalo electrons reach as much as 20–200 keV (Wang et al. 2010). The feasibility of sodium separation from different types of host minerals due to space weathering near the Sun should be studied further. Our simulations of sodium sublimation and outgassing from Phaethon should be considered a "best-case scenario" of how Phaethon's activity could behave in optimum conditions. Under such circumstances, Na-driven comet-like activity seems feasible. However, continued research is needed to better understand potential production mechanisms of pure sodium, the strength of activity at lower abundances of sodium or when the sodium content is present in different mineral phases, and the effect of surface-layer processing on Phaethon during multiple orbits.

3. Laboratory Analysis

3.1. Meteorite Sample

We obtained a sample of meteorite material to test its reaction to high temperatures in order to determine the capability of sodium to be a driver of activity on small solar system bodies in a material analogous to Phaethon. For this study, we used centimeter-scale units of the Allende (CV3) meteorite, totaling 67.94 g in mass. At the present, there is no

established analog for Phaethon or any Pallas-like B-type asteroid in our meteorite collection. We know that Phaethon has a geometric visible albedo of 10%–16% (Hanuš et al. 2018a; Taylor et al. 2019; Masiero et al. 2019), which is lower than that of S-type asteroids that have been linked to the ordinary chondrite (OC) meteorites. This link was established by the return of samples from Itokawa by the Hayabusa mission (Yoshikawa et al. 2015), and thus we can exclude OCs as a possible analog. Phaethon is unlikely to be a metal body and shows no similarity with Vesta or its family, which excludes iron or howardite eucrite diogenite (HED) meteorites as possible analogs. As carbonaceous chondrites are the largest group that cannot be excluded, we use them for our study.

The choice of Allende specifically was driven by the need to acquire a relatively large quantity of material away from the original surface (and any potential terrestrial weathering) for our proposed destructive analysis; as Allende was a large fall, it was the most accessible carbonaceous chondrite for our study. Allende is classified as a CV3 chondrite and thus likely not a perfect match for Phaethon, which has been suggested to be related to CM chondrites (Hanuš et al. 2018b) or CK4 chondrites (Clark et al. 2010), although these associations are based on weak spectral features and so are uncertain. Should Phaethon be a CK4 type, the metamorphic history experienced by CK4 chondrites would mean that plagioclase would be the most common sodium-bearing mineral instead of sodalite and nepheline for Allende (Greenwood et al. 2010). However, the goal of this work is to test the behavior of carbonaceous chondrites to heating similar to what Phaethon experiences, specifically their sodium-bearing minerals. Future work, motivated by the results of this study, will extend this investigation to other carbonaceous meteorites that may be better analogs for Phaethon.

Previous work has shown that Allende contains an average of 0.46% of Na_2O, making it the second most abundant volatile element after sulfur at ~ 2.1 wt% (Jarosewich et al. 1987). In contrast, evolved comets like 67P/Churyumov–Gerasimenko have a 5%–80% mass fraction of cometary volatiles in their nucleus (Fulle et al. 2017; Choukroun et al. 2000), in this case water ice. This two-orders-of-magnitude difference would imply that if sodium volatilization does spur activity on objects close to the Sun, it would be expected to be at a much lower level than the activity seen for comets, but potentially detectable with sufficient sensitivity. Water volatilization would be expected to be significantly stronger, so sodium-driven activity would only be possible for objects like Phaethon that do not contain subsurface water.

To prepare the meteorite material for our tests, we crushed the sample by hand in a mortar and pestle made of corundum, and filtered the material through a 250 μm sieve, reserving a few larger chips for microscopic analysis. We prepared 14 aliquants of the powdered sample, each 0.5 g in mass. We reserved the remaining material for future analysis. All tools and storage containers were cleaned and rinsed with methanol prior to handling the sample.

3.2. Experimental Setup

The proposed temperature (1123 K) of Na release by sublimation of sodalite by Kasuga et al. (2006) was derived from the 50% condensation temperature of Na in the solar nebula by Lodders (2003). However, sodalite is a secondary mineral formed during metasomatic alteration of chondrites,
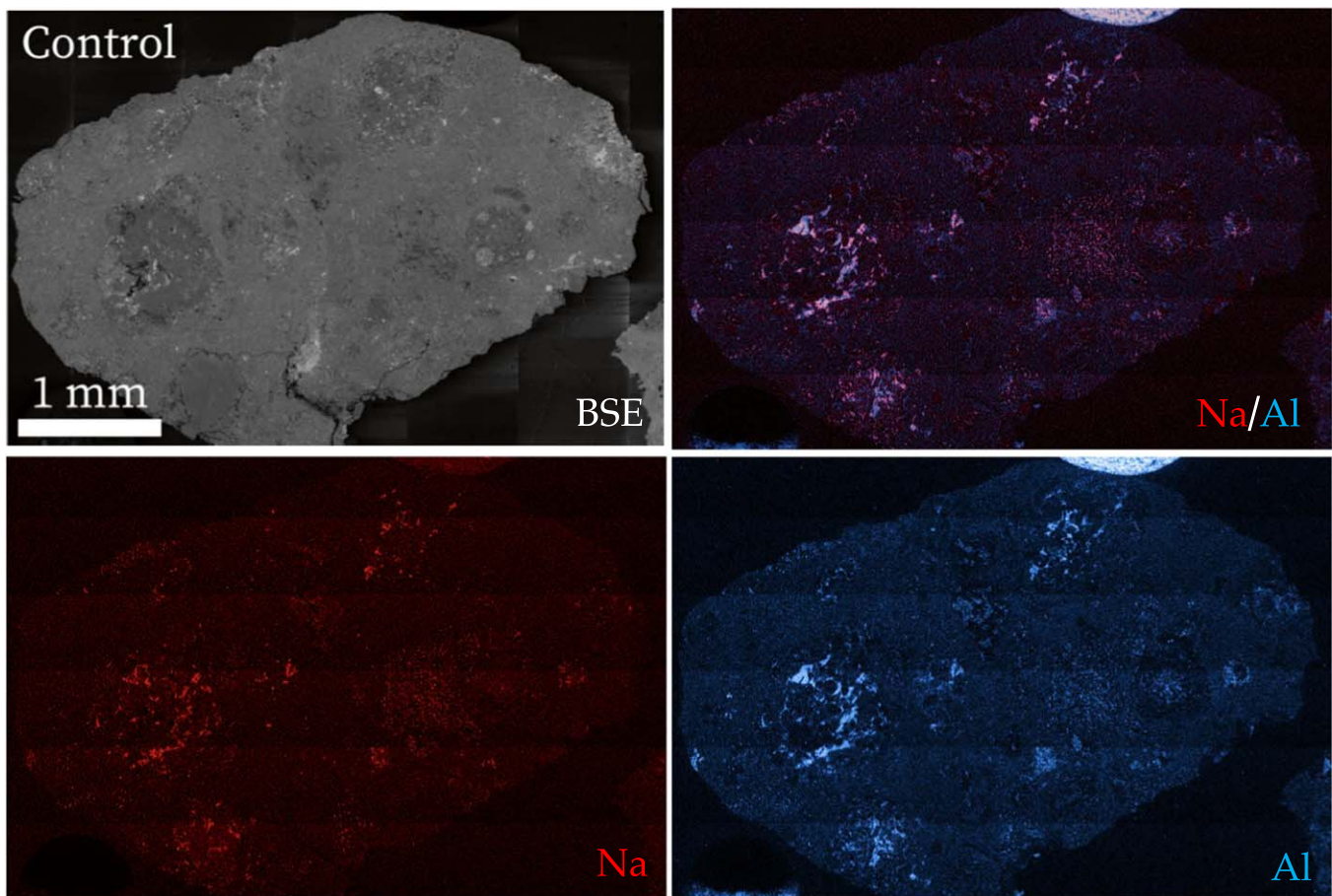
Figure 3. Backscattered electron (BSE) image and the EDS Na and Al maps of the control sample (Chip G). The Na and Al maps for the control and the heated chip (Figure 4) were plotted on the same intensity scale to enable direct comparison. An interactive figure is provided in the online version of this article, showing an overlay of the Na and Al maps, with a slide bar allowing the viewer to change between them.

meaning that the use of the condensation temperature of Na may not be fully applicable in this case. Previous heating experiments of Allende and Murchison for Na loss were conducted at 1323–1623 K (Wulf et al. 1995). To evaluate if sublimation occurs at lower temperatures as proposed by Kasuga et al. (2006) due to the prevailing conditions on asteroids near the Sun compared to at their formation, we tested a range of temperatures designed to span the peak heating experienced by NEOs such as Phaethon. We heated samples of powder and chips at each of the following temperatures: 573 K (300 °C), 673 K (400 °C), 773 K (500 °C), 873 K (600 °C), 973 K (700 °C), and 1073 K (800 °C). We also held powder and chip samples in reserve as controls.

Each aliquant was placed in a cleaned ceramic crucible and then placed inside an oven at room temperature. The oven took approximately 30–60 minutes to ramp up to the target temperature and then 30–120 minutes to cool down (with higher peak temperatures taking longer to both heat and cool). The aliquant was held at peak temperature for 1 hr. For simplicity, we refer to the heated samples using the peak temperature. The oven was at ambient atmosphere during heating, which is much more oxidizing than the heating in vacuum experienced by Phaethon. Wulf et al. (1995) and Sossi et al. (2019) showed that Na volatility increases with decreasing oxygen fugacity. Thus, any change we observed from our experiment provides a lower bound on the Na loss in vacuum. The timescale of heating and cooling experienced by these samples roughly corresponds to one diurnal cycle of

Phaethon (which has a rotation period of 3.6 hr). Future work will investigate heating in a vacuum to better simulate the environment Phaethon experiences.

After the experiment, one chip fragment from the control sample (G) and each heated aliquant (A–F) were chosen randomly to prepare a grain mount. These chips were embedded in EpoCure™ epoxy and subsequently ground and polished to generate a smooth flat surface for later analyses. Grinding materials included SiC, diamond, and alumina. Except for diamond and alumina in pore spaces and cracks, contamination by grinding materials to the samples was not significant enough to be noticeable.

Chips A–G were imaged on a Hitachi SU3500 scanning electron microscope (SEM) equipped with an Oxford 150 energy dispersive X-ray spectroscopy detector at the Jet Propulsion Laboratory (JPL). Backscattered electron images (BSE) and maps were collected at 15 kV with a spot current intensity of 70. Each full-area EDS map mosaic is composed of a compilation of areas that were imaged and analyzed at 150× magnification with image resolution of 1024 and four frames per map area. EDS full-grain map mosaic images were converted from text image files to png files in Fiji, and images were colorized and combined to generate overlay maps using Photoshop.

Precise compositions of different phases in the unheated Chip G and heated Chip F were analyzed using a JEOL JXA-8200 electron probe microanalyzer (EPMA) at the California
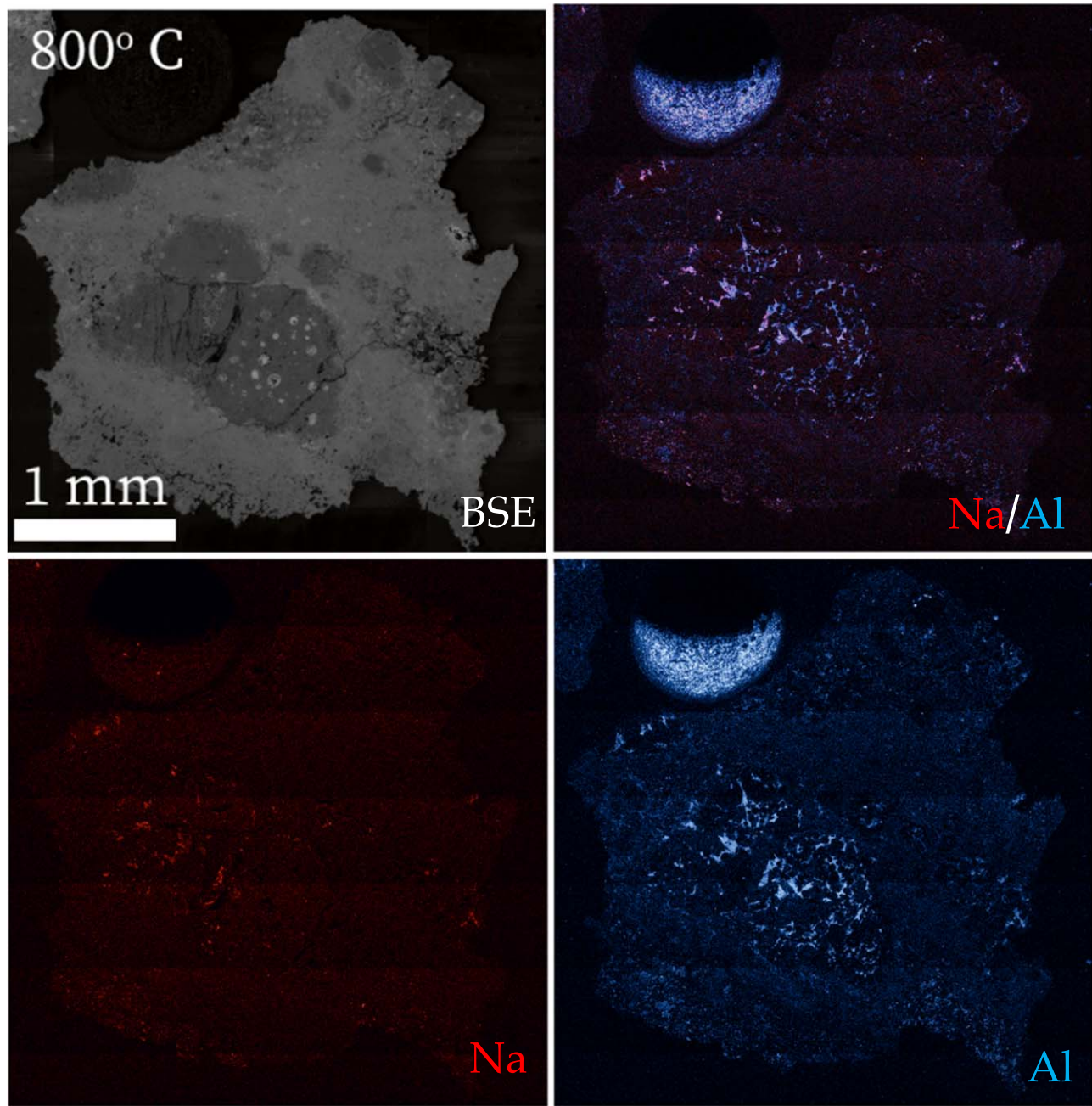
Figure 4. Same as Figure 3, for the sample heated at 1073 K (Chip F). The bright, rounded feature near the top left of the EDS maps is an artifact from an epoxy bubble and not part of the sample under investigation. An interactive figure is provided in the online version of this article, showing an overlay of the Na and Al maps, with a slide bar allowing the viewer to change between them.

Institute of Technology. A focused electron beam of 10 kV and 10 nA was used. The Kα lines of Si, Ti, Al, Cr, Fe, Mn, Mg, Ca, Na, K, and Cl were counted for 20 s, with Na being counted first to avoid significant Na loss during analyses. The mean atomic number (MAN) method (Donovan & Tingle 1996) was used for the background corrections. Standards for analysis include natural and synthetic materials.

3.3. Experimental Results

The EDS full-chip maps of aluminum and sodium for the unheated and 1073 K chips are presented in Figures 3 and 4. These maps show the distribution of elements present in detectable abundances (>0.1 wt%). The EDS map of the unheated Chip G illustrates a close spatial association of Na with Al and Si but not with Cl, consistent with an interpretation that Na is present in aluminosilicates, likely nepheline and feldspar. Comparison of the EDS maps of the heated chips with the control sample shows that only the sample heated to 1073 K (Chip F) displays lower Na abundances than the control sample, whereas Al and Si are comparable to the control sample. The areas around the phases that should be sodium-rich in the heated sample do not show any increase in sodium content in the EDS maps, suggesting that the reaction that occurred was decomposition rather than Fickian diffusive loss. This suggests that Na-rich aluminosilicates in Chip F lost Na when heated to 1073 K (800 °C).

8

Table 2
Electron Probe Microanalyzer Results—Nepheline/Groundmass

| Oxide | Chip F | | | | | | Chip G | | | | K95[a] | | | W11[a] | K95[a] | | |
	Nepheline/Groundmass						Nepheline				Nepheline				Groundmass		
SiO_2	42.6	43.9	43.2	45.7	43.1	44.3	42.7	42.7	42.3	41.4	42.5	42.2	42.8	43.1	44.9	41.7	38.2
TiO_2	<0.03	<0.03	0.05	<0.03	<0.03	<0.03	0.07	<0.03	<0.03	<0.03	<0.03	<0.03	<0.03	<0.03	0.27	0.32	0.36
Al_2O_3	37.0	36.4	33.3	37.1	35.9	33.8	35.9	35.2	35.3	35.3	34.6	32.8	33.7	35.7	26.3	28.2	27.3
Cr_2O_3	<0.03	0.04	<0.03	<0.03	<0.03	<0.03	0.06	0.09	<0.03	<0.03	<0.03	0.16	<0.03	<0.03	0.65	0.09	0.25
FeO	0.81	0.93	1.40	1.45	1.42	2.30	0.43	0.48	1.49	1.18	0.24	0.13	0.27	0.21	1.45	4.77	4.19
MnO	0.11	0.06	0.03	0.39	<0.02	<0.02	0.02	<0.02	<0.02	<0.02	0.07	0.06	<0.02	0.04	0.03	0.00	0.14
MgO	2.64	2.71	3.20	3.34	4.71	6.78	0.10	0.30	0.27	0.21	0.20	0.19	0.01	0.09	3.49	5.89	4.83
CaO	4.32	2.93	5.85	2.88	2.79	3.16	2.21	2.51	2.29	2.20	2.10	2.18	1.08	0.96	8.33	2.04	4.88
Na_2O	11.4	12.8	11.7	9.84	10.2	9.09	16.9	17.5	15.0	15.8	17.9	18.2	19.2	17.4	13.2	14.6	14.2
K_2O	0.44	0.49	0.37	0.29	0.24	0.17	2.18	2.12	1.92	1.91	2.09	1.82	1.93	1.50	1.27	1.56	0.01
Cl	<0.02	<0.02	<0.02	<0.02	<0.02	0.08	<0.02	<0.02	0.02	0.04	0.02	<0.02	<0.02	<0.02	<0.02	<0.02	4.66
Total	99.4	100.2	99.1	101.0	98.3	99.6	100.5	101.0	98.6	98.1	99.7	97.7	98.9	99.0	99.8	99.2	99.0

Note.
[a] References from the literature: K95 = Kimura & Ikeda (1995), W11 = Wasserburg et al. (2011).

Table 3
Electron Probe Microanalyzer Results—Sodalite

Oxide	Chip F						Chip G			K95[a]		W11[a]
SiO_2	39.1	40.6	39.2	42.0	39.9	36.9	38.2	36.3	36.7	36.3	36.0	39.1
TiO_2	<0.03	0.04	<0.03	<0.03	<0.03	0.08	<0.03	<0.03	<0.03	<0.03	<0.03	<0.03
Al_2O_3	32.4	33.9	34.4	35.7	34.4	32.7	31.7	31.6	32.3	30.9	31.1	35.2
Cr_2O_3	<0.03	0.05	0.03	<0.03	0.05	0.04	<0.03	<0.03	0.06	<0.03	<0.03	<0.03
FeO	1.41	0.86	1.50	1.56	1.57	2.10	0.67	1.08	1.49	0.74	0.70	0.18
MnO	<0.02	<0.02	0.09	0.14	0.04	0.22	0.03	<0.02	<0.02	<0.02	<0.02	<0.02
MgO	0.84	1.77	1.18	1.43	2.38	3.23	0.15	0.09	0.39	0.10	0.17	0.08
CaO	2.96	3.42	0.53	0.79	1.13	1.47	0.44	0.54	1.37	0.08	0.17	0.07
Na_2O	11.3	11.2	8.4	6.6	7.4	11.5	18.4	23.5	22.3	25.4	24.4	17.9
K_2O	0.10	0.07	0.03	0.05	0.06	0.14	0.12	0.03	0.04	0.04	0.02	<0.02
Cl	5.52	5.61	7.89	7.72	6.72	6.76	6.89	7.32	6.78	6.68	7.03	7.10
Total	93.6	97.6	93.4	96.0	93.6	95.1	96.6	100.5	101.4	100.2	99.6	99.6

Note.
[a] References from the literature: K95 = Kimura & Ikeda (1995), W11 = Wasserburg et al. (2011).

EPMA data for Chip F and Chip G are listed in Table 2 for the nepheline and groundmass phases and Table 3 for the sodalite phases. Pyroxene and plagioclase about 20 μm away from the Na-rich phases did not show high Na content, further supporting that the Na-rich phases did not lose Na through Fickian diffusion. Note that after heating, sodalite and nepheline have been altered to different mineral phases. For simplicity, we refer to them as heated sodalite and nepheline. Low oxide totals of heated sodalite in Chip F (<97.6 wt%) could be caused by Na loss, fine grains, or bad polish. Sodalite in unheated Chip G is also fine-grained and similarly polished, but oxide totals are acceptable. Therefore, we regard the bad totals of heated sodalite to be mainly due to Na loss. Although these low totals are below expected values for complete analyses, we included them here to show the changes in Na contents. Compared to unheated sodalite in Chip G, heated sodalite Chip F clearly shows lower Na_2O and higher Al_2O_3, CaO, and MgO, although Cl and FeO appear to be similar between those two chips (Figure 5). It is unclear why Cl did not show comparable changes, though it may be due to the low overall Cl content (see the Appendix, Figures A1 and A2). Further studies are needed to investigate the behavior of Cl in sodalite during heating. The heated nepheline in Chip F contains much higher MgO and CaO than unheated ones in Chip G, although Al_2O_3 contents are comparable between the two chips (Figure 6). An increase in refractory components indicates that a small amount of mafic phases was annealed with the heated sodalite. However, the dilution effects by this mixing are inadequate to explain the decrease in Na. The heated nepheline in Chip F may be groundmass, given that its MgO and CaO contents are similar to altered groundmass in Kimura & Ikeda (1995). Regardless, Na_2O contents in heated nepheline in Chip F are much lower than unheated nepheline in Chip G or unheated groundmass in Kimura & Ikeda (1995). Using average values, heated sodalite and nepheline in Chip F show maximum Na loss of 55% and 35%, respectively. These results demonstrate that at peak temperature (1073 K) for a relatively short time (~1 hr), Na can be lost from nepheline and sodalite. Although the changes in Chip F may be due to thermal decomposition under our experimental conditions, these results show that heating under vacuum may facilitate the generation of Na vapor, which will be explicitly tested in future work.

4. Discussion

Nepheline in carbonaceous chondrites is a secondary mineral formed through thermal metamorphism or metasomatism of primary materials (e.g., Ikeda & Kimura 1995; Kimura & Ikeda 1995; Krot et al. 1998). Another mineral, sodalite $[Na_4(Si_3Al_3)O_{12}Cl]$, could also be a source for Na volatilization. Nepheline and sodalite in carbonaceous chondrites typically occur as accessory phases in trace quantities, but samples with high abundances are present (e.g., Wasserburg et al. 2011). Surface materials on Phaethon could possibly contain significant abundances of nepheline or sodalite that would contribute to the observed vaporization event.

Previous heating experiments of Allende conducted by Wulf et al. (1995) reached higher temperatures than those in our study, with samples heated for longer times. As such, those experiments probed a different regime of thermal exposure than our work, more appropriate to the study of silicate vaporization. In those experiments, powder and chips of Allende and Murchison were heated to 1323–1623 K (1050 °C–1350 °C) under different oxygen fugacities. Results by Wulf et al. (1995) showed that more Na is lost under reduced conditions. Na vaporization can be written in a generalized reaction form: $\frac{1}{2}$ Na_2O (s or l) = Na (g) + $\frac{1}{4}$ O_2 (g). Thus, the lower oxygen fugacity drives this reaction toward the right-hand side. At 1323 K, only 26% bulk Na was lost from samples heated in air. In contrast, our experiments showed up to 55% loss of Na from sodalite and nepheline. We attribute this difference to the fact that Na is hosted in this sample in both refractory grains (albite) and secondary phases (nepheline and sodalite). While our analysis focused only on the secondary phase minerals, the bulk analysis contains both refractory and secondary phases and therefore would have a more muted sodium loss. More importantly, our experimental results demonstrate that Na can be lost from secondary minerals such as nepheline in a short heating period that is predicted from the thermophysical modeling above. Thus, the observed losses combined with the predictions from models support our theory that sodium can be a driver of activity on small, near-Sun asteroids.

The OSIRIS-REx spacecraft has observed particles recently launched in short-term stable orbits around the carbonaceous NEO (101955) Bennu (Lauretta et al. 2019). These centimeter-scale objects were observed to be ejected from the surface, typically in the late afternoon on low-energy orbits. Numerous
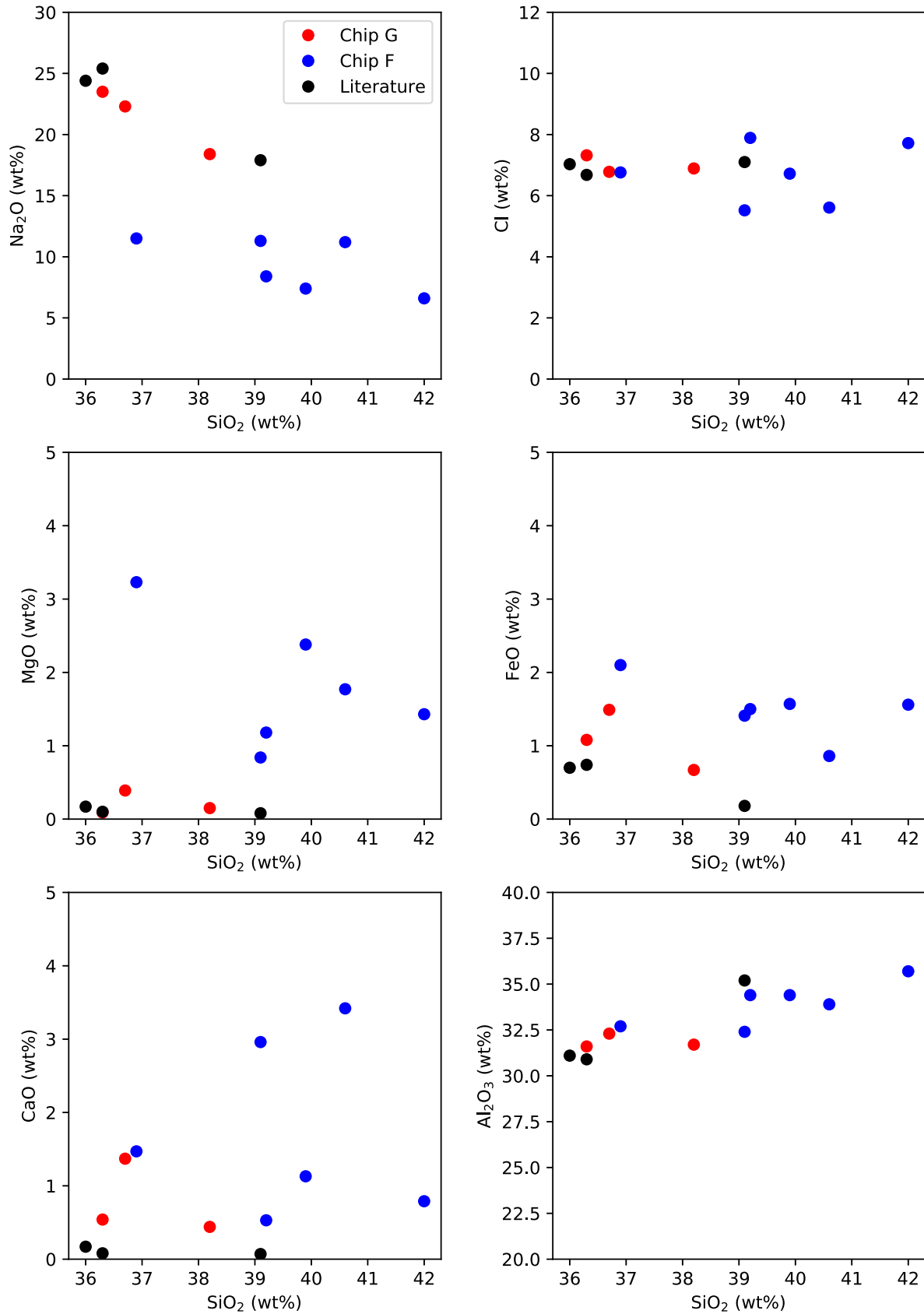
Sodalite

Figure 5. EPMA data for sodalite phases comparing the fractional composition of various oxides to the SiO₂ weight percentage. Shown are the control chip (Chip G), the heated chip (Chip F), and data from the literature from Kimura & Ikeda (1995) and Wasserburg et al. (2011). Data show raw values that have not been renormalized to 100%.
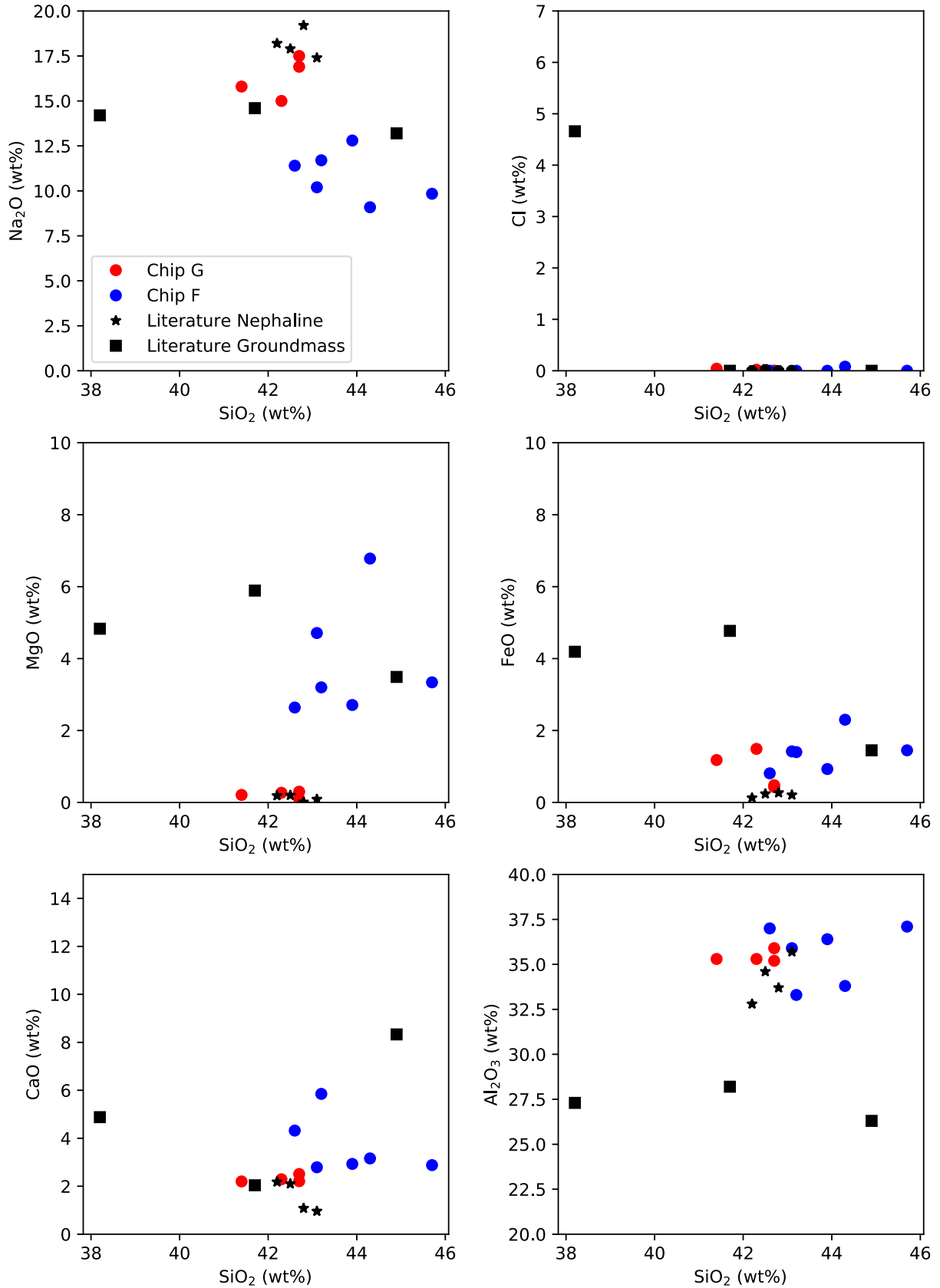
Nepheline/Groundmass

Figure 6. Same as Figure 5, but showing phases composed of nepheline or groundmass.

possible ejection mechanisms including thermal fracturing, electrostatics, and phyllosilicate dehydration were investigated, but no direct cause was confirmed. The surface of Bennu does not reach the same peak temperatures as that of Phaethon, making sodium volatilization unlikely to be responsible for these events. Still, Bennu stands as another interesting example of unexpected forms of activity on NEOs in addition to Phaethon.

Recent work by MacLennan et al. (2021) describes the long-term evolution of the thermal history of Phaethon, showing that it experiences cyclical changes to its maximum heating from the Sun. Based on those results, Phaethon currently is just past the peak of its ∼18 kyr heating cycle, which would imply that sodium volatilization should be ramping down. This heating history is consistent with Phaethon having had higher levels of sodium-driven activity in the past few thousand years. This could then explain how Phaethon created the Geminid meteor stream in the recent past but has a present-day activity insufficient to produce it. Additional models by MacLennan et al. (2021) predict that asteroid (155140) 2005 UD, which may have been formed from an earlier splitting of Phaethon, is at the beginning of a new heating cycle, and we would expect sodium volatilization to increase over the next ∼5 kyr from a currently quiescent state.

When considering the broader NEO population, Granvik et al. (2016) demonstrated that there is a significant lack of low-albedo asteroids with very low-perihelion distances. They attribute this lack of small, dark objects to extreme thermal events, though for many of the asteroids with low perihelia the time to reach these orbits is nontrivial. We would therefore not expect a breakup scenario like what is observed for low-perihelia comets, as these NEOs spend a significant time heated to well above the temperature for ice sublimation. Any existing ice must be deeply buried and would not respond rapidly (or catastrophically) to heating. Sodium volatilization, then, could act as the needed trigger to remove some of the dehydrated surface material and expose enough ice-rich subsurface to trigger the catastrophic breakups needed to explain the observations of Granvik et al. (2016).

5. Conclusions

Both our theoretical thermophysical modeling and laboratory analyses indicate that sodium has the potential to mobilize dust on the surface of small bodies when other more volatile agents (e.g., water) are not present. This mechanism could then explain the activity seen on objects with very low perihelia such as Phaethon. However, this activity would depend strongly on the mineral phases present and the specific surface geology of these objects.

Further work is needed to make more specific predictions for Phaethon, including conducting heating experiments in a vacuum and using meteorite materials that are closer analogs to Phaethon than Allende. Likewise, future investigations of larger quantities of heated analog material would enable testing of the efficiency of deposition of a pure sodium layer that could later be rapidly triggered to cause outgassing. Results of these

studies then would lead to improved models of dust mobilization on the Phaethon's surface.

The DESTINY+ mission that is currently being pursued by JAXA (Arai et al. 2018, 2019) will provide in situ observations of Phaethon for the first time. These data may allow us to determine if, and to what extent, sodium contributes to the observed activity on Phaethon. If Phaethon's dust emission is indeed driven by sodium desorption, this mechanism provides another avenue for mass loss on small solar system bodies, especially those close to the Sun.

More broadly, simulations of the orbital evolution of the whole NEO population by Marchi et al. (2009) indicate that approximately 2% of the current NEO population had or will have a perihelion distance within 0.1 au at some point in their dynamical lifetimes. This means that sodium volatilization would not be expected to be restricted to just Phaethon, but instead may drive activity on a small but important subset of the whole NEO population. Investigations of other asteroids with small perihelia will allow us to determine the extent to which this novel form of activity is present among the asteroids.

Appendix
Supplemental Figures

Maps of Cl location within the chips for the control sample (Figure A1) and heated sample (Figure A2), for comparison with the sodium maps.
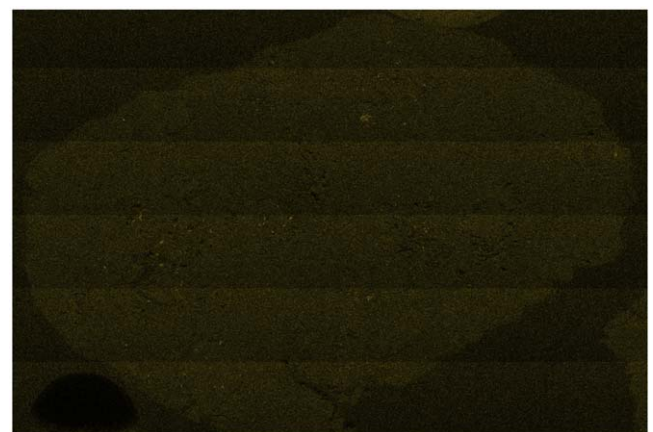

Figure A1. EDS Cl map of the control sample (Chip G), for comparison with the Na and Al maps shown in Figure 3.

Figure A2. EDS Cl map of the sample heated at 1073 K (Chip F), for comparison with the Na and Al maps shown in Figure 4.

ORCID iDs

Joseph R. Masiero ⬤ https://orcid.org/0000-0003-2638-720X

References

Abe, S., Ogawa, T., Maeda, K., et al. 2020, P&SS, 194, 105040
Arai, T., Kobayashi, M., Ishibashi, K., et al. 2018, LPSC, 49, 2570
Arai, T., Kobayashi, M., Ishibashi, K., et al. 2019, LPICo, 82, 6497
Asplund, M., Grevesse, N., Sauval, A. J., & Scott, P. 2009, ARA&A, 47, 481
Čapek, D., & Borovička, j. 2009, Icar, 202, 361
Cassidy, T., Merkel, A., Burger, M., et al. 2015, Icar, 248, 547
Choukroun, M., Altwegg, K., Kührt, E., et al. 2000, SSRv, 216, 44
Clark, B. E., Ziffer, J., Nesvorny, D., et al. 2010, JGR, 115, E06005
Davidsson, B. J. R. 2021, MNRAS, 505, 5654
Davidsson, B. J. R., Birch, S., Blake, G. A., et al. 2021, Icar, 354, 114004
Davidsson, B. J. R., & Skorov, Y. V. 2002, Icar, 159, 239
Delbo, M., Libourel, G., Wilkerson, J., et al. 2014, Natur, 508, 233
Donovan, J. J., & Tingle, T. N. 1996, MiMic, 02, 1
Fougere, N., Altwegg, K., Berthelier, J.-J., et al. 2016, MNRAS, 462, S156
Fulle, M., Della Corte, V., Rotundi, A., et al. 2017, MNRAS, 469, S45
Garenne, A., Beck, P., Montes-Hernandez, G., et al. 2014, GeCoA, 137, 93
Golubeva, L. F., Shestopalov, D. I., & Kvaratskhelia, O. I. 2020, arXiv:2001.00789
Granvik, M., Morbidelli, A., Jedicke, R., et al. 2016, Natur, 530, 303
Greenwood, R. C., Franchi, I. A., Kearsley, A. T., & Alard, O. 2010, GeCoA, 74, 1684
Gustafson, B. 1989, A&A, 225, 533
Hanuš, J., Delbo', M., Pokorny, P., et al. 2018b, EPSC, 13, 1386
Hanuš, J., Delbo', M., Vokrouhlický, D., et al. 2016, A&A, 592, A34
Hanuš, J., Vokrouhlický, D., Delbo, M., et al. 2018a, A&A, 620L, 8
Huebner, W. F. 1970, A&A, 5, 286
Ikeda, Y., & Kimura, M. 1995, AMR, 8, 97
Jarosewich, E., Clark, R. S., & Barrows, J. N. 1987, SmCES, 27, 1
Jewitt, D., Hsieh, H., & Agarwal, J. 2015, in Asteroids IV, ed. F. E. DeMeo & W. F. Bottke (Tucson, AZ: Univ. Arizona Press), 221
Jewitt, D., & Li, J. 2010, AJ, 140, 1519
Kasuga, T., Watanabe, J., & Ebizuka, N. 2005, A&A, 438, L17
Kasuga, T., Yamamoto, T., Kimura, H., & Watanabe, J. 2006, A&A, 453, L17
Kimura, M., & Ikeda, Y. 1995, AMR, 8, 123
Krot, A. N., Petaev, M. I., Scott, E. R. D., et al. 1998, M&PS, 33, 1065
Lauretta, D. S., Hergenrother, C. W., Chesley, S. R., et al. 2019, Sci, 366, 3544
Li, J., & Jewitt, D. 2013, AJ, 145, 154
Lodders, K. 2003, ApJ, 591, 1220
Macke, R. J., Consolmagno, G. J., & Britt, D. 2011, M&PS, 46, 1842
MacLennan, E., Toliou, A., & Granvik, M. 2021, Icar, 366, 114535
Marchi, S., Delbo, M., Morbidelli, A., et al. 2009, MNRAS, 400, 147
Masiero, J., Wright, E. L., & Mainzer, A. 2019, AJ, 158, 97
Mekler, Y., Prialnik, D., & Podolak, M. 1990, ApJ, 356, 682
Notsu, K., Onuma, N., Nishida, N., & Nagasawa, H. 1978, GeCoA, 42, 903
Prialnik, D. 1992, ApJ, 388, 196
Robie, R. A., Hemingway, B. S., & Takei, H. 1982, AmMin, 67, 470, https://pubs.geoscienceworld.org/msa/ammin/article-abstract/67/5-6/470/41384/Heat-capacities-and-entropies-of-Mg2SiO4-Mn2SiO4?redirectedFrom=fulltext
Rubin, A. E. 1997, M&PS, 32, 231
Russell, D. P., & Sanders, M. 1994, REDS, 132, 119
Ryabova, G. O. 2018, MNRAS, 479, 1017
Shoshany, Y., Prialnik, D., & Podolak, M. 2002, Icar, 157, 219
Sossi, P., & Fegley, B., Jr 2018, RvMG, 84, 393
Sossi, P. A., Klemme, S., O'Neill, H. S. C., et al. 2019, GeCoA, 260, 204
Takir, D., Kareta, T., Emery, J., et al. 2020, NatCo, 11, 2050
Tancredi, G., Rickman, H., & Greenberg, J. M. 1994, A&A, 286, 659
Taylor, P. A., Rivera-Valentín, E. G., Benner, L. A. M., et al. 2019, P&SS, 167, 1
Wang, L., Yang, L., He, J., et al. 2010, ApJL, 803, 2
Wasserburg, G. J., Hutcheon, I. D., Aléon, J., et al. 2011, GeCoA, 75, 4752
Wulf, A. V., Palme, H., & Jochum, K. P. 1995, P&SS, 43, 451
Yomogida, K., & Matsui, T. 1983, JGR, 88, 9513
Yoshikawa, M., Kawaguchi, J., Fujiwara, A., & Tsuchiyama, A. 2015, in Asteroids IV, ed. F. E. DeMeo & W. F. Bottke (Tucson, AZ: Univ. Arizona Press), 397
Yu, L. L., Ip, W. H., & Spohn, T 2019, MNRAS, 482, 4243